JOURNAL OF ENGINEERING SCIENCES

Volume 11, Issue 1 (2024)

Veselovska N., Sivak R., Paladiychuk Y., Bandura V., Telyatnik I., Bohatiuk M., Savkiv V., Edl M. (2024). Kinematic characteristics of deformed porous structures. Journal of Engineering Sciences (Ukraine), Vol. 11(1), pp. D44–D53. https://doi.org/10.21272/jes.2024.11(1).d6

Kinematic Characteristics of Deformed Porous Structures

Veselovska N.[1][0000-0001-9399-6721], Sivak R.[2][0000-0002-7459-2585], Paladiychuk Y.[1][0000-0002-9925-0987], Bandura V.[3][0000-0001-8074-3020], Telyatnik I.[1][0000-0002-2998-1506], Bohatiuk M.[1][0000-0002-2318-3781], Savkiv V.[1][0000-0002-3733-3963], Edl M.[4*][0000-0003-0761-7882]

[1] Vinnytsia National Agrarian University, 3, Sonyachna St., 21000 Vinnytsia, Ukraine;
[2] Polissia National University, 7, Staryi Blvd., 10002 Zhytomyr, Ukraine;
[3] National University of Life and Environmental Sciences of Ukraine, 15, Heroiv Oborony St., 03041 Kyiv, Ukraine;
[4] University of West Bohemia, 2732/8, Univerzitní St., 301 00, Pilsen, Czech Republic

Article info:
Submitted: September 18, 2023
Received in revised form: February 15, 2024
Accepted for publication: March 1, 2024
Available online: March 14, 2024

***Corresponding email:**
edl@fst.zcu.cz

Abstract. Experimental and computational methods of studying the stress state in the plastic region are characterized by various methods and accuracy of measurements, methods of mathematical processing of experimental information, and interpretation of results. The experimentally determined kinematics as a starting point is the most widely used method to study the stress-strain state in the plastic region. When studying the process of plastic deformation of porous blanks, the model of a rigid-plastic isotropic-strengthening porous body with a loading surface that has the shape of an ellipsoid with semi-axes. It depends on the amount of porosity and the ratio of the associated flow law as a mechanical model of the material. In the axisymmetric extrusion of porous blanks, the viscoplasticity method was used to determine the field of flow velocities based on the results of experimental studies. R-functions were applied to approximate experimentally obtained values. The problem of finding approximations was formulated in a variational statement. Cubic splines of one argument were used to interpolate functions. As a result, an approach was proposed, which consists of a particular sequence of calculating the derivatives of the coordinates of the nodes in time in combination with the R-functions approach. All the calculations were performed in Euler variables, eliminating the need to switch from Lagrangian variables and simplifying the solution. Additionally, this method allowed for working with an irregular and non-rectangular grid in areas with any shape of boundaries. This approach is more effective from the point of view of the approximation's accuracy and the speed of calculations. Finally, the equation for calculating the porosity in the volume of the deformable workpiece based on the information about the distortion of the dividing grid elements was obtained. For stationary axisymmetric processes, a technique was developed that allowed for replacing the calculation of the accumulated deformation of the base material along the deformation trajectory by integration over the region. A technique was developed for determining the stress-strain state at unstable and stable stages of axisymmetric plastic deformation of porous blanks. The calculation results were compared based on the proposed experimental and calculation techniques and the finite element method.

Keywords: porous body, spline interpolation, non-stationary state, axisymmetric deformation, visioplasticity method, Euler coordinates, Lagrangian coordinates.

1 Introduction

Methods of obtaining information about deformation processes experimentally known to our time are limited to determining displacements, deformations, sometimes flow velocities, and specific stress functions. None of the known experimental methods allow directly determining stress at arbitrary points of a deformable body. An essential step in determining the stress state is obtaining reliable information about the kinematics of the process. If the kinematics (displacement, flow velocity) is known, then it is possible to determine the components of the tensors of strains and velocities, their degree of deformation, and the stress intensity from the flow curve or hardness measurement method. Next, the stress deviator components can be calculated using the deformation

theory of plasticity or flow theory, and then, integrating the equilibrium equation, the hydrostatic stress [1].

To assess the deformability of porous materials in pressure treatment processes, it is necessary to have information about the dependence of plasticity on various factors. This approach is widely used in phenomenological theories of failure of compact materials.

The basis of ideas about the exhaustion of metal plasticity is the physical model of the accumulation of damage in plastic deformation. Plastic deformation is known to be accompanied by loosening of metal, and the amount of loosening is generally proportional to the degree of deformation. From this point of view, the destruction process becomes a kinetic process of development, accumulation, and connection of micropores and microcracks. Simultaneously, as plastic loosens, the "healing" of defects is facilitated by an increase in temperature and hydrostatic pressure. The predominance of nucleation of defects over their "healing" at a particular stage of plastic deformation contributes to the initiation of microcracks, which cause destruction [2, 3].

During plastic deformation of porous bodies, damage accumulation is more complicated. In this case, plastic loosening co-occurs with the material compaction process. The determining destruction factor is not "looseness" or porosity in general but the development and accumulation of micropores and microcracks, mainly along those planes corresponding to the most significant linear shift or the most considerable linear deformation in the base material. In addition, the pores in the material are sinks for dislocations, which slows down the rate of damage accumulation. In macroscopic experiments, it is impossible to separate the processes of compaction and loosening of the material.

However, currently, enough experimental data have been accumulated, and it follows that the intensity of each process depends on many factors.

2 Literature Review

The coordinate grid method is most effectively used to study the deformed state on the surface and inner regions of the workpieces. It has been established experimentally that, for example, during pressing and drawing of cylindrical blanks, the meridional cross-sections of which have a grid applied, the distribution of deformations and stresses in them is the same as in wholes [4, 5], since the normal stresses between the layers in the meridional cross-section are compressive, and there are no tangents.

The macrostructure detection and microstructure methods can also be considered methods of obtaining natural grids [6, 7]. When the system of geometric marks on the deforming surface becomes dense enough, the moiré method can be considered when developing the method of coordinate grids. Instead of grids, systems of dots applied, for example, by the kerning method, are also sometimes used.

Ratios for calculating deformations on curved grids were first obtained [8] for cases when the initial square grid, drawn on the main plane, turns into a parallelogram after deformation. More general formulas are obtained when the initial cell has the shape of a parallelogram, which is especially important in the step-by-step study of shape change processes. Methods of this type are very versatile. Disadvantages include time-consuming measurements, low accuracy of measurements of small deformations, and obtaining results averaged within the boundaries of the cell. In addition, these techniques give significant errors if the sides of the cell are strongly distorted after deformation.

Along with the direct study of the shape change of the elementary cell, the measurement technique can be built on the step-by-step measurement of the coordinates of points (e.g., grid nodes and labels), that is, the determination of the field of displacements for a given time and the subsequent determination of the field of deformation rates. Next, the transition to the stressed state is performed according to the relations of the flow theory [9].

Experimental information contains systematic errors caused by the measurement method and random errors caused by the casual spread of the measured values. Mathematical processing should separate factors from the investigated dependence. At the same time, it is assumed that the investigated function is continuous and differentiable, and random factors do not possess this property. In addition to the requirements of good convergence to the approximating objects, it is necessary to satisfy the boundary conditions known from the theoretical analysis of the process (conditions on the axis of symmetry, border of rigid, and plastic zones).

Algorithms based on approximating experimental data by power polynomials and Fourier series have good versatility [10, 11]. Although a good approximation to the smoothing function is achieved, the calculation of the derivatives is unsatisfactory since the approximating function in the calculation area has a certain number of extremums unrelated to the features of the measured values.

Spline functions [12] are free from many disadvantages of polynomial approximation and allow for the easy fulfillment of boundary conditions [13]. However, to construct a spline, boundary conditions are required at all boundaries of the region, and since they are not known everywhere, they have to be set subjectively, which reduces the accuracy of calculations.

In works [14], a model of a nonlinear narrow-elastic medium was proposed to study the extrusion of powder materials through axisymmetric matrices, which made it possible to formulate and solve a boundary value problem.

Simultaneously, experimental data obtained on full-scale samples using coordinate grids was used to determine the field of velocities in the center of deformation.

The main drawback of the considered approaches is that it is assumed that the stress deviators based on the curvature of the dividing grid or the results of other experimental measurements are determined accurately. In fact, due to the above reasons, deviators contain errors that cannot always be estimated.

In [10], it is proposed to look for solutions in the form of functions that exactly satisfy the equilibrium equation, the plasticity condition, and the boundary conditions. At the same time, partial solutions obtained by independent integration of each equilibrium equation are used. However, partial solutions can differ very significantly. The approach [15] should be considered more reasonable, where it is proposed to exactly satisfy the equilibrium equations in the nodes of the calculation grid with an inevitable weakening of the requirements for the fulfillment of the plasticity condition.

In [16], a method for calculating stresses based on experimentally determined kinematics is proposed based on the theory of R-functions, the advantage of which is that it allows the boundary conditions and equilibrium equations to be satisfied identically at any point of the region with a complex boundary shape. At the same time, certain deviations from the condition of plasticity and flow equations are allowed. Approximation of deviators obtained based on experimental information about the kinematics of the plastic deformation process is performed by statically permissible stress fields. This method is up-and-coming and opens the way to increase the accuracy of stress calculation.

When processing arrays of experimental data, the choice of approximations plays an important role. It is most natural to use functions of three arguments for approximations. For example, in [16], it is recommended that quasi-interpolation L-splines be used for this purpose. However, this approach has some limitations: the output grid must be rectangular and uniform, and the shape of the meridional section must be rectangular. Significant difficulties are also associated with transferring from Lagrange variables to Euler ones. This approach is necessary when calculating stresses since the equilibrium equations are more easily integrated into the Euler variables and for a more precise presentation of the obtained results.

An approach in which splines of one argument (by time) and two arguments (by coordinates at each stage) are used for approximation and differentiation has become widespread. Such techniques have fewer limitations than those described above. In this case, the original grid may be irregular (but rectangular), and the meridional cross-section may have a shape other than rectangular. In this case, the sequence of approximations of the coordinates of the nodes has a noticeable effect on the results of the calculations. The advantages of this approach include the possibility of independence of node coordinate measurements at different stages. Simultaneously, in this case, it is necessary to approximate time derivatives by coordinates, which leads to significant errors. The time approximation is less accurate due to the small number of stages, and the derivatives have already been determined with some errors.

3 Research Methodology

3.1 The traditional approach

With a known field of strain rates, the hydrostatic stress can also be determined as follows [17]. Let's decompose the stress tensor into deviatoric and spherical parts

$$\sigma_{ij} = S_{ij} + \sigma\delta_{ij}, \quad (1)$$

and present the equilibrium equation in the following form:

$$\frac{\partial(S_{ij}+\sigma\delta_{ij})}{\partial x_j} = \frac{\partial\sigma}{\partial x_j}\delta_{ij} + \frac{\partial S_{ij}}{\partial x_j} = 0. \quad (2)$$

Let's substitute the expression in (2) instead of S_{ij}:

$$S_{ij} = \frac{2F}{\dot{\varepsilon}_u}\dot{e}_{ij} \quad (3)$$

and let's represent the components of the strain rate tensor through the components of the velocity vector.

As a result, we will get a system of three differential equations:

$$\frac{\partial\sigma}{\partial x_j}\delta_{ij} + \frac{\partial}{\partial x_j}\left[\frac{2F}{\dot{\varepsilon}_u}\left(\frac{\partial v_i}{\partial x_j} + \frac{\partial v_j}{\partial x_i}\right)\right] = 0, \quad (4)$$

to which the incompressibility equation should be added:

$$\dot{\varepsilon}_{ij}\delta_{ij} = \frac{\partial v_i}{\partial x_i} = 0. \quad (5)$$

A system of four differential equations (4) and (5) with respect to the three components of the velocity vector and the average hydrostatic pressure is obtained. They should be supplemented with boundary conditions for the velocities:

$$\sigma_{ij}\nu_j = (\sigma\delta_{ij} + S_{ij})\nu_j = \left[\sigma\delta_{ij} + \frac{2F}{\dot{\varepsilon}_u}(v_{i,j} + v_{j,i})\right]\nu_j = S_i. \quad (6)$$

Therefore, the stressed state is calculated from the deformed state, considering the ratios of the theory of plasticity. The desired stress field must satisfy the equilibrium equation, the plasticity condition, the flow law, and the boundary conditions. The unambiguity of the solution is ensured if the velocity field satisfies conditions (4) and (5).

When determining stresses by kinematics, which does not satisfy condition (4), integrating equilibrium equations along discontinuous paths can lead to a significant difference between the solutions, which in individual zones can reach hundreds of percent [18].

3.2 The proposed approach

According to the results of experimental studies, it was established that in the case of plastic deformation of sintered porous materials, the most reliable results can be obtained if the deformation of the base material accumulated before the moment of failure is used as a measure of plasticity [19, 20]:

$$\Gamma_{op} = \int_0^{t_p}\dot{\gamma}_0 d\tau, \quad (7)$$

where t_p – the time of deformation to failure; $\dot{\gamma}_0$ – the deviator's intensity and the base material's deformation rates.

In general, the ultimate deformation of the base material depends on various factors:

$$\Gamma_{op} = f\left(x_i, c_j, \eta, \mu_\sigma, T, \dot{\Gamma}, \alpha_{ij}, \theta\right), \quad (8)$$

where x_i – parameters that allow for considering the influence of the chemical composition and sintering conditions; c_j – influence of the structure; η and μ_σ – influence factors of the stress state scheme; T – influence of temperature; $\dot{\Gamma}$ – rate of deformation; α_{ij} – influence of load non-monotonicity; θ – impact of porosity.

For cold, monotonous processes of pressure treatment, which occur at low deformation rates, the dependence (8) is reduced to the form:

$$\Gamma_{op} = f\left(x_i, c_j, \eta, \mu_\sigma, \theta\right). \quad (9)$$

The chemical composition and structure characterize the natural plasticity of the material. The influence of the rest is determined by experimental studies conducted according to the relevant programs. As a result, dependence (9) is reduced to the form:

$$\Gamma_{op} = f\left(\eta(\Gamma_0, \theta), \mu_\sigma(\Gamma_0, \theta)\right), \quad (10)$$

where Γ_0 – the accumulated deformation of the base material at this moment.

Thus, the stress state scheme is an important factor in determining plasticity for cold processes of pressure treatment of porous bodies.

The dependence of plasticity on the stress state scheme will be described by the surface of ultimate plasticity, which is constructed in coordinates: the ultimate stress-strain state indicators Γ_{Or}.

As one of the indicators of the stress state, we can accept an indicator that has proven itself well in assessing the stress state of compact materials:

$$\eta = \frac{I_1(T_\sigma)}{\sqrt{I_2(D_\sigma)}} = \frac{3p}{\sigma_u} = \frac{3p}{\sqrt{\frac{3}{2}}\tau} = \sqrt{6}\frac{p}{\tau};\ \sigma_u = \sqrt{\frac{3}{2}}\tau, \quad (11)$$

where σ_u – stress intensity.

The concept of the stress state indicator of the base material can be introduced to evaluate the stress state scheme of porous sintered materials:

$$\eta_0 = \sqrt{6}\frac{p_0}{\tau_0}. \quad (12)$$

Since

$$p = p_0(1-\theta), \quad (13)$$

and then after considering [21]:

$$\tau_0^2 = \frac{p^2}{f_2(\theta)(1-\theta)} + \frac{\tau^2}{f_1(\theta)(1-\theta)}, \quad (14)$$

expression (12) can be reduced as follows:

$$\eta_0^2 = \frac{6P^2}{(1-\theta)^2\tau_0^2} = \frac{6P^2}{(1-\theta)\left[\frac{P^2}{f_2(\theta)} + \frac{\tau^2}{f_1(\theta)}\right]} = \frac{6\left(\frac{P}{\tau}\right)^2}{(1-\theta)\left[\left(\frac{P}{\tau}\right)^2\frac{1}{f_2} + \frac{1}{f_2}\right]},$$

and finally:

$$\eta_0 = \eta\sqrt{\frac{f_1(\theta)}{(1-\theta)\left[\frac{1f_1(\theta)}{6f_2(\theta)}\eta^2+1\right]}}. \quad (15)$$

After considering [22]:

$$\alpha(\theta) = \frac{1}{6}\frac{f_1(\theta)}{f_2(\theta)}, \quad (16)$$

expression (15) is reduced to the following form:

$$\eta_0 = \eta\sqrt{\frac{f_1(\theta)}{(1-\theta)(\alpha\eta^2+1)}}. \quad (17)$$

The stress state indicator η_0 considers the influence of hydrostatic pressure, which significantly affects the plasticity of a porous body, as well as the influence of the intensity of tangential stresses, which determine the plastic flow of the material.

When studying the process of plastic deformation of porous blanks, the model of a rigid-plastic isotropic-strengthening porous body with a loading surface that has the shape of an ellipsoid with semi-axes that depend on the porosity is taken as a mechanical model of the material. Simultaneously, the stress intensity in the base material of the porous body is determined by formula (14). From it, according to the associated flow law, the following tensor is obtained:

$$\dot{e}_{ij} - \frac{1}{3}\delta_{ij}\dot{e} = \frac{\dot{\gamma}}{\tau}\left(\sigma_{ij} - \delta_{ij}p\right), \quad (18)$$

as well as a scalar ratio

$$pf_1(\theta)\dot{\gamma} = \tau f_2(\theta)\dot{e} \quad (19)$$

between stress tensor components σ_{ij} and strain rates $\dot{e}_{ij}$.

The accumulated deformation of the base material is taken as a measure of deformation strengthening of a porous body:

$$\Gamma_0 = \int_0^t \dot{\gamma}_0(\tau)d\tau. \quad (20)$$

The porosity functions $f_1(\theta)$ and $f_2(\theta)$, as well as the flow curve $\tau_0(\Gamma_0)$ for the base material [22], are determined as follows:

$$f_1(\theta) = (1-\theta)^{3.5}; \quad (21)$$

$$f_2(\theta) = 0.549\frac{(1-\theta)^{4.36}}{\theta^{0.86}}; \quad (22)$$

$$\tau_0 = -15 + 83.73\Gamma_0^{0.186}. \quad (23)$$

From equations (14) and (19), the formulas for the connection of kinematic and static quantities are obtained:

$$\tau = \tau_0 f_1(\theta)\frac{\dot{\gamma}}{\dot{\gamma}_0}; \quad (24)$$

$$p = \tau_0 f_2(\theta)\frac{\dot{e}}{\dot{\gamma}_0}. \quad (25)$$

They can be applied to evaluate the intensity of the stress deviator and the average stress in a porous body [21].

From relations (14), (18)–(25), to determine the stress-strain state of a porous body on a deformed coordinate grid, it is necessary to determine the following:

1) the field of components of flow velocities of body particles v_i;

2) the field of strain rate components:

$$\dot{e}_{ij} = \frac{1}{2}\left(\frac{\partial v_i}{\partial x_j} + \frac{\partial v_j}{\partial x_i}\right); \quad (26)$$

3) the field of accumulated deformation of the base material Γ_0;

4) intensity field of stress deviator (yield strength) of base material τ_0;

5) porosity field θ in the plastic region;

6) field of stress deviator components S_{ij} and stress tensor σ_{ij}.

These stages correspond to the requirements presented in [23–27].

4 Results

During the axisymmetric extrusion of porous blanks, the field of flow velocities was determined by the visioplasticity method based on the results of experimental studies. In the experimental studies, blanks with a diameter of d_0 = 20 mm and a length of l_0 = 46 mm were used with a known initial porosity θ_0 and a rectangular mesh with a step approximately equal to 2 mm along the *z*-axis.

The sample was deformed in a matrix with an angle at the apex of the cone of the matrix α. In the stationary mode, the force *P* and the speed of the punch v_0 were determined.

The coordinates of the (l, m)-th node, where $l = 1, 2, ..., L$ and $m = 1, 2, ..., M$ (Figure 1), before deformation (in Lagrangian coordinates) were denoted $z_{0_{l,m}}$ and $r_{0_{l,m}}$, and after deformation (in Eulerian coordinates) – $z_{l,m}$ and $r_{l,m}$, respectively.

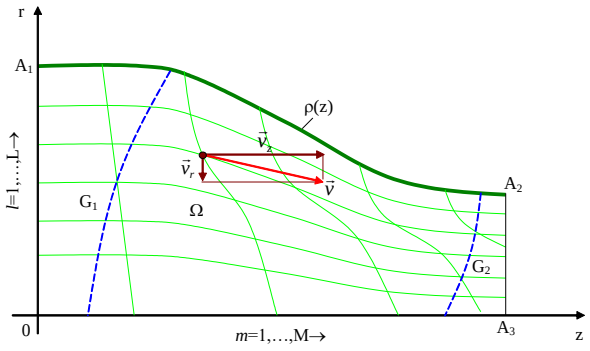

Figure 1 – Design scheme of the kinematics on a curved grid

In this way, experimental functions of Euler coordinates from Lagrangian coordinates were obtained at the grid nodes:

$$\bar{z}_{l,m} = \bar{z}\left(z_{0_l}, r_{0_m}\right); \; \bar{r}_{l,m} = \bar{r}\left(z_{0_l}, r_{0_m}\right), \quad (27)$$

or in Lagrangian coordinates from Euler coordinates:

$$z_{0_{l,m}} = z_0(z_l, r_m); \; r_{0_{l,m}} = r_0(z_l, r_m). \quad (28)$$

Since the flow velocities of material particles v_z and v_r for stationary deformations can be calculated using the formulas [7]:

$$v_z = v_0 \frac{\partial z}{\partial z_0}; \quad (29)$$

$$v_z = \frac{v_0}{\Delta}\frac{\partial r_0}{\partial r}; \quad (30)$$

$$v_r = v_0 \frac{\partial r}{\partial z_0}; \quad (31)$$

$$v_z = \frac{v_0}{\Delta}\frac{\partial r_0}{\partial r}, \quad (32)$$

where

$$\Delta = \frac{\partial z_0}{\partial z}\frac{\partial r_0}{\partial r} - \frac{\partial z_0}{\partial r}\frac{\partial r_0}{\partial z}. \quad (33)$$

To simplify the calculations using formulas (29)–(32), it can be assumed that v_0 = 1. Also, the linear dimensions can be normalized so that the radius of the matrix container is equal to one, for which the coordinates of the nodes z_0, r_0, *z*, and *r* should be multiplied by $\lambda = \frac{1}{R_0}$.

The values of flow velocities obtained as a result of calculations will have to be multiplied by v_0, and the values of the components of the strain rate tensor $\dot{e}_{ij}$ – by λv_0.

Since it is more convenient to perform stress calculations in Euler coordinates (equilibrium equations have a more straightforward form), we will also calculate the kinematics in Euler coordinates, which eliminates the need to move from one coordinate to another and, in addition, allows us to present the results more clearly (on a deformed sample). Formulations (30) and (32) will be used in further calculations.

To construct approximations dependencies $z_0(z, r)$ and $r_0(z, r)$ for experimentally obtained function values $\bar{z}_{0_{l,m}}$ and $\bar{r}_{0_{l,m}}$, a technique based on the methods of the theory of R-functions [16] was used. It was successfully applied for studies of the stress-strain state of non-porous materials.

The main advantages of this method include the ability to obtain solutions that identically satisfy the boundary conditions for regions with a complex boundary configuration.

The problem of finding approximations z_0 and r_0 was formulated in the variational statement [21]:

$$\sum_{l=1}^{L\Sigma}\sum_{m=1}^{M\Sigma}\alpha_{l,m}^{(a)}\left(z_{0_{l,m}} - \bar{z}_{0_{l,m}}\right)^2 + \delta_a \iint_{\Omega}\left[\left(\frac{\partial^2 z_0}{\partial z^2}\right)^2 + 2\left(\frac{\partial^2 z_0}{\partial z \partial r}\right)^2 + \left(\frac{\partial^2 z_0}{\partial r^2}\right)^2\right] d\Omega \to min; \quad (34)$$

$$\sum_{l=1}^{L\Sigma}\sum_{m=1}^{M\Sigma}\alpha_{l,m}^{(b)}\left(r_{0_{l,m}} - \bar{r}_{0_{l,m}}\right)^2 + \delta_b \iint_{\Omega}\left[\left(\frac{\partial^2 r_0}{\partial z^2}\right)^2 + 2\left(\frac{\partial^2 r_0}{\partial z \partial r}\right)^2 + \left(\frac{\partial^2 r_0}{\partial r^2}\right)^2\right] d\Omega \to min. \quad (35)$$

where Ω – the solution area of the problem (meridional section of the workpiece) (Figure 1); δ_a, δ_b, $\alpha_{l,m}^{(a)}$, and $\alpha_{l,m}^{(b)}$ – weighting factors that allow for ensuring the proper ratio between the smoothness of the functions $\bar{z}_{0_{l,m}}$ and

$\bar{r}_{0_{l,m}}$, as well as the approximation to the experimentally obtained values $\bar{z}_{0_{l,m}}$ and $\bar{r}_{0_{l,m}}$, respectively. They also consider various errors in determining the experimental functions at different points of the area.

Let's consider the approximations z_0 and r_0 in the following forms:

$$z_0 = \sum_{k=1}^{N} c_k \beta_k ; \quad (36)$$

$$r_0 = r \sum_{k=1}^{N} c_k \beta_k . \quad (37)$$

where c_k – arbitrary numerical coefficients; β_k – elements of any complete system of functions.

In this case, shifts of B-splines of Schoenberg [16] are used.

According to the theory of R-functions, expressions (36) and (37) are called structures. They make it possible to satisfy the boundary conditions identically. In the considered problem, the structure ensures the boundary condition on the symmetry axis (37).

The substitution of equations (36) and (37) to formulas (34) and (35), respectively, and minimization by the coefficients of c_k leads in each case to a system of linear algebraic equations with respect to c_k, where the n-th equation for z_0 takes the following forms:

$$\sum_{k=1}^{N} C_k \{\sum_{l=1}^{L} \sum_{m=1}^{M} \alpha_{l,m}^{(a)} z_{0l,m}(\beta_k) z_{0l,m}(\beta_n) + \delta_a \iint_{\Omega} [6 \frac{\partial^2 z_0(\beta_k)}{\partial z^2} \frac{\partial^2 z_0(\beta_n)}{\partial z^2} + 2 \frac{\partial^2 z_0(\beta_k)}{\partial z \partial r} \frac{\partial^2 z_0(\beta_n)}{\partial z \partial r} + + \frac{\partial^2 z_0(\beta_k)}{\partial r^2} \frac{\partial^2 z_0(\beta_n)}{\partial r^2}] d\Omega\} = \sum_{l=1}^{L} \sum_{m=1}^{M} \alpha_{l,m}^{(a)} \bar{z}_{0l,m} z_{0l,m}(\beta_n); \quad (38)$$

$$\sum_{k=1}^{N} C_k \{\sum_{l=1}^{L} \sum_{m=1}^{M} \alpha_{l,m}^{(a)} r_{0l,m}(\beta_k) r_{0l,m}(\beta_n) + \delta_a \iint_{\Omega} [6 \frac{\partial^2 r_0(\beta_k)}{\partial r^2} \frac{\partial^2 r_0(\beta_n)}{\partial r^2} + 2 \frac{\partial^2 r_0(\beta_k)}{\partial z \partial r} \frac{\partial^2 r_0(\beta_n)}{\partial z \partial r} + + \frac{\partial^2 r_0(\beta_k)}{\partial z^2} \frac{\partial^2 r_0(\beta_n)}{\partial z^2}] d\Omega\} = \sum_{l=1}^{L} \sum_{m=1}^{M} \alpha_{l,m}^{(a)} \bar{r}_{0l,m} r_{0l,m}(\beta_n). \quad (39)$$

The system of equations for determining the function r_0 can be obtained by replacing z_0 with r_0 in (38).

Figure 2 shows the meridional section of the sample with a curved coordinate grid after extrusion. Figure 3 presents the results of calculating the particle flow rate. Figure 4 presents the components of the strain rate tensor.

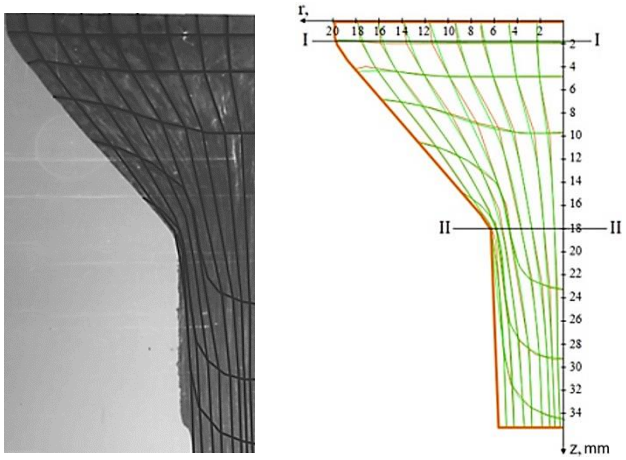

a b

Figure 2 – Meridional cross-section of a porous sample: a – distortion of the dividing grid of the sample after extrusion; b – dividing grid lines obtained after the experiment ( ) and after calculations using equations (36)–(39) ( )

According to the obtained results, the curved grid obtained as a result of the experiment and using the experimental and calculation methods almost coincide entirely.

The analysis of the obtained results shows that the difference in calculations for specific kinematic characteristics according to the proposed experimental and calculation methods and using the finite element method is especially noticeable at the workpiece's meridional cross-section II–II. This can cause significant errors in stress state calculations.

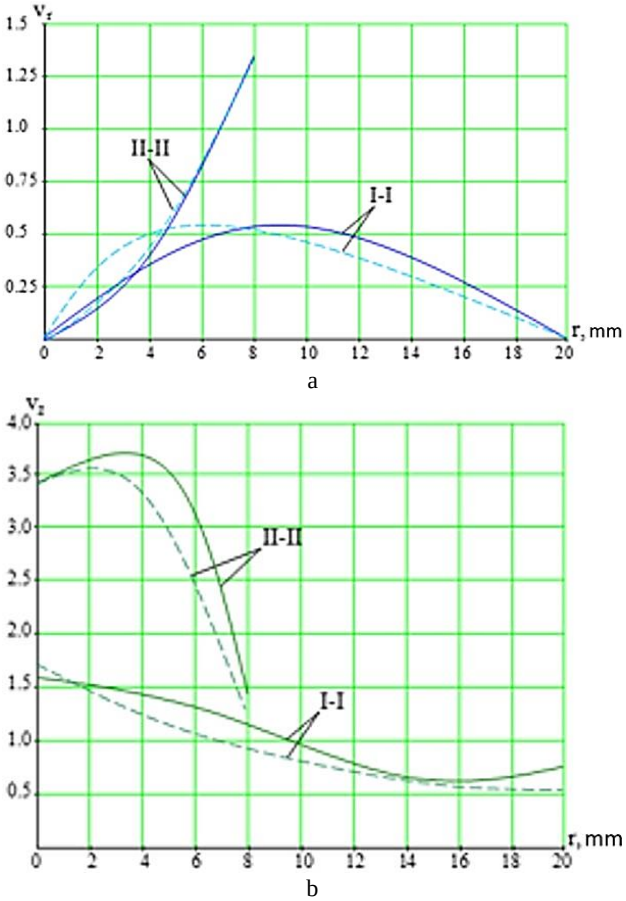

Figure 3 – Particle flow velocities v_r (a) and v_z (b) in the cross-sections I–I and II–II (Figure 2b) during sample extrusion: solid line – experimental and calculation method; dashed line – theoretical solution

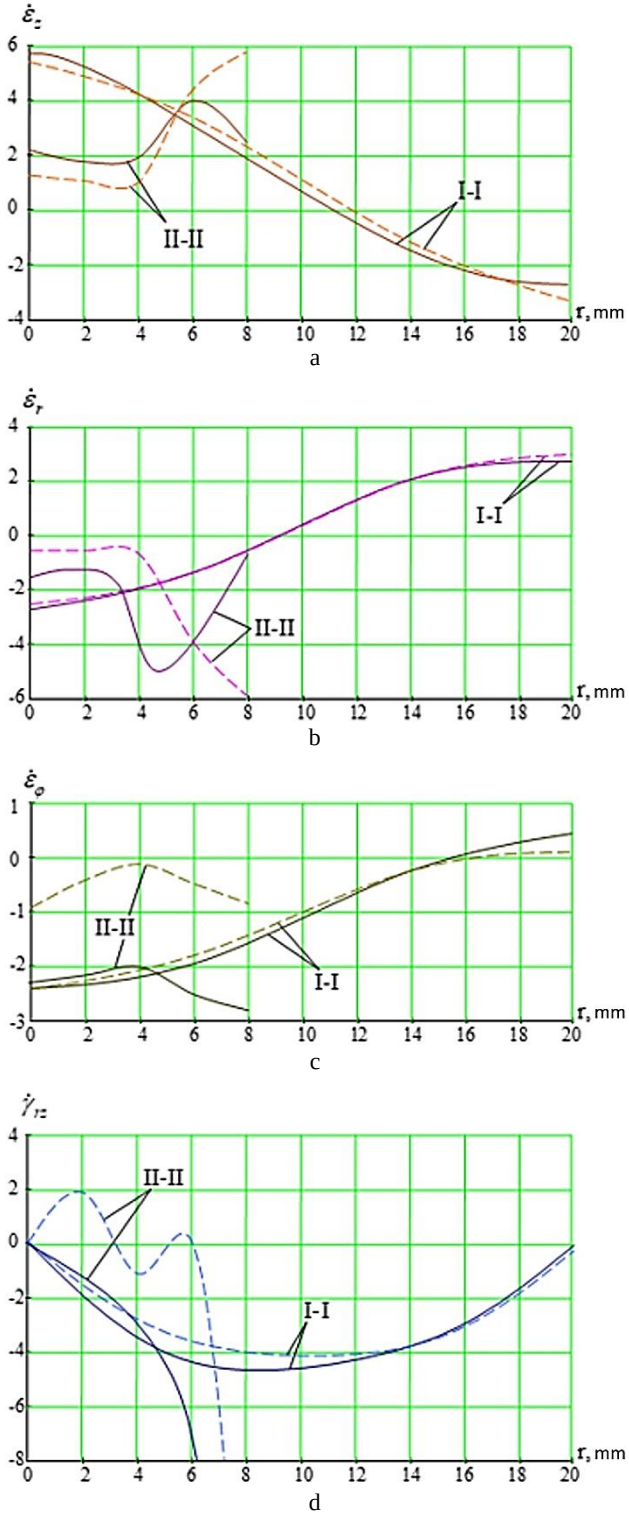

Figure 4 – Components of the strain rate tensor $\dot{\varepsilon}_z$ (a), $\dot{\varepsilon}_r$(b), $\dot{\varepsilon}_\phi$ (c), and $\dot{\gamma}_{rz}$ (d) in sections I–I and II–II (Figure 2b) while extruding the sample: solid line – experimental and calculation method; dashed line – theoretical solution

After substituting the solutions of the resulting systems of equations to (36) and (37), we obtain the approximations z_0 and r_0. Then, the particles' velocities can be determined using formulas (30) and (32).

Further, using dependencies (26), strain rate intensities $\dot{\gamma}_0$ and $\dot{\gamma}$ are as follows:

$$\dot{\gamma}_0^2 = \frac{f_2(\theta)\dot{e}^2}{1-\theta} + \frac{f_1(\theta)\dot{\gamma}^2}{1-\theta}; \quad (40)$$

$$\dot{\gamma} = \sqrt{\left(\dot{e}_{ij} - \frac{1}{3}\dot{e}\delta_{ij}\right)\left(\dot{e}_{ij} - \frac{1}{3}\dot{e}\delta_{ij}\right)} = \sqrt{\frac{2}{3}}\,\dot{\varepsilon}_u. \quad (41)$$

The considered technique is also suitable for determining the components of the strain rate tensor of solid bodies for which porosity $\theta_0 = 0$.

The magnitude of the accumulated deformation in the base material $\Gamma_0(r, z)$ can be calculated directly by formula (20). Simultaneously, integral (20) is calculated along the trajectory of particle deformations.

The method proposed in [16] can be proposed to calculate $\Gamma_0(r, z)$. This technique is based on the theory of R-functions and allows for replacing integration along the trajectory with integration over the area. This approach reduces the calculation error and simplifies the algorithm.

After differentiating (20) with respect to t and considering considering $\frac{dz}{dt} = v_z$ and $\frac{dr}{dt} = v_r$, an equation in partial derivatives satisfied by Γ_0 can be obtained:

$$\frac{\partial \Gamma_0}{\partial z} v_z + \frac{\partial \Gamma_0}{\partial r} v_r = \dot{\gamma}_0. \quad (42)$$

For a unique solution of equation (42), it is necessary to set the boundary conditions along the line that coincides with the trajectory. For example, the accumulated plastic deformation $\Gamma_0 = 0$ at the boundary of the elastic and plastic zone G_1 at the entrance to the matrix:

$$\Gamma_0|_{G_1} = 0. \quad (43)$$

To obtain an approximate solution of problem (42) with the boundary condition (43), an equivalent variational problem is stated:

$$\iint_\Omega \left(\frac{\partial \Gamma_0}{\partial z_0} v_z + \frac{\partial \Gamma_0}{\partial r} v_r - \dot{\gamma}_0\right)^2 d\Omega \to min, \quad (44)$$

and the structure will be taken as follows:

$$\Gamma_0 = \omega_1 \sum_{k=1}^{N} c_k \beta_k, \quad (45)$$

where ω_1 – a function that defines the boundary of G_1 and is constructed according to the R-functions method so that $\omega_1|_{G_1} = 0$, and for points belonging to the region Ω: $\omega_1 > 0$.

After substituting (45) to (44) and minimizing the obtained functional with respect to s_k, a system of linear algebraic equations can be obtained, the n-th equation of which takes the following form:

$$\sum_{k=1}^{N} c_k \iint_\Omega \left[\frac{\partial \Gamma_0(\beta_k)}{\partial z} v_z + \frac{\partial \Gamma_0(\beta_k)}{\partial r} v_r\right]\left[\frac{\partial \Gamma_0(\beta_n)}{\partial z} v_z + \frac{\partial \Gamma_0(\beta_n)}{\partial r} v_r\right] d\Omega = \iint_\Omega \dot{\gamma}_0 \left[\frac{\partial \Gamma_0(\beta_n)}{\partial z} v_z + \frac{\partial \Gamma_0(\beta_n)}{\partial r} v_r\right] d\Omega. \quad (46)$$

By substituting the solution of the system of equations (46) to (45), the value of Γ_0 can be obtained.

Figure 5 presents the calculation results of the accumulated deformation in the base material.

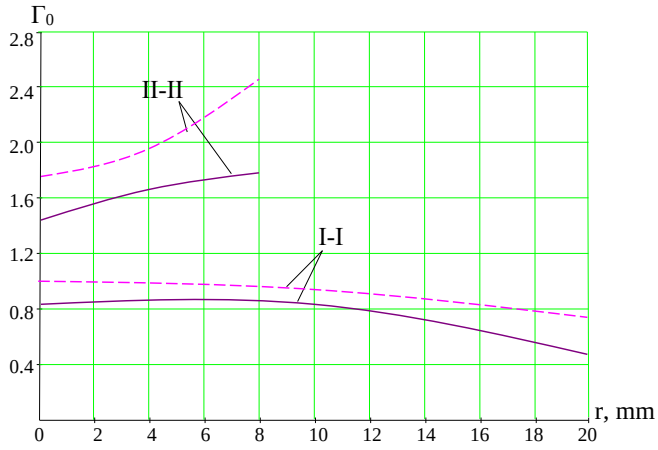

Figure 5 – The accumulated deformation of the base material in the cross-sections I–I and II–II (Figure 2b) during sample extrusion: solid line – experimental and calculation method; dashed line – theoretical solution

The obtained results also indicate a particular discrepancy between the calculations of the accumulated deformation of the base material according to the proposed experimental and calculation techniques using the finite element method.

Since the position of border G_1 is not exactly known, the line $z = 0$ was taken as the border, and then $\omega_1 = z$.

To study the non-stationary unsteady (initial stage) extrusion of porous bodies, the same samples as for the previously considered stationary process were used, made from PZh4M2 powder with the same step of the coordinate grid on the meridional cross-section along with the z-axis.

The samples were pressed through a matrix with a compression of 64 % in m stages. The initial blank is considered to be at the zero stage. After each stage, the nodes' coordinates of the grid were fixed.

As before, calculating the kinematics based on the known nodes' coordinates for the deformed grid is reduced to finding approximations $z(z_0, r_0, t)$ and $r(z_0, r_0, t)$ of the experimentally found coordinates $\bar{z}_{l,m}$ and $\bar{r}_{l,m}$, where l is the node number, and m is the number of the deformation stage.

5 Discussion

The approach in which splines of one argument (by time) and splines of two arguments (by coordinates at each stage) are used for approximation and differentiation has a significant impact on the results of calculations in the case when the original grid may be non-uniform (but rectangular), and the meridional section may have a shape other than rectangular. Then it can be first approximated the coordinates of the nodes at each stage: $z_m(z_0, r_0, t_m)$ and $r_m(z_0, r_0, t_m)$, and then approximated the values of the coordinates and their derivatives along z_0 and r_0 in the nodes $z_1(t)$, $r_1(t)$.

However, more effective, from the point of view of the accuracy of the approximation, as well as the speed of calculations, is the approach in which the derivatives of the coordinates of the nodes in time are first calculated (that is, the flow velocities of the material particles are determined), and then their derivatives in terms of coordinates z_0, r_0. The article uses this approach in combination with the methods of the theory of R-functions, and all calculations are performed in Euler variables, which eliminates the need to switch from Lagrangian variables to Euler ones and simplifies the solution of the problem. In addition, this method allows working with an irregular and non-rectangular grid in regions with any shape of borders [21].

Approximate values of the flow velocities of the material particles in the lth node of the grid were calculated using the following ratios:

$$\bar{v}_{z_{l,m}} = \frac{dz_l(t_m)}{dt};\ \bar{v}_{r_{l,m}} = \frac{dr_l(t_m)}{dt}, \tag{47}$$

where $z_1(t)$ and $r_1(t)$ – approximations of the experimental values of the node coordinates $\bar{z}_{l,m}$ and $\bar{r}_{l,m}$, respectively, which were built using cubic spline functions of one argument.

The time function t can be determined from the displacement of the tool S and its speed v_0:

$$t = \frac{S}{v_0}. \tag{48}$$

If v_0=const, then in formulas (47), it is convenient to use S instead of t, then instead of values $\bar{v}_z$ and $\bar{v}_r$ we obtain their values normalized to v_0.

To construct approximations of the velocity values $v_z(z, r, t_m)$ and $v_r(z, r, t_m)$, obtained by formulas (47) in Euler variables, a technique based on the methods of the theory of R-functions was used, which is a development of the technique used previously to study the kinematics of deformation in a stationary process.

The problem of finding approximations was formulated in a variational statement (for each stage):

$$\sum_{l=1}^{L\Sigma} \alpha_1 \left(f_1 - \bar{f}_1\right)^2 + \delta \iint_\Omega \left[\left(\frac{\partial^2 f}{\partial z^2}\right)^2 + 2\left(\frac{\partial^2 f}{\partial z \partial r}\right)^2 + \left(\frac{\partial^2 f}{\partial r^2}\right)^2\right] d\Omega \to min, \tag{49}$$

where $f(z, r)$ – an approximating function; $\bar{f}_1$ – the value of the approximated function in nodes; α_1 and δ – weight factors that allow for ensuring the necessary relationship between the smoothness of the function f and the approximation to the values of $\bar{f}$, as well as considering the accuracy of determining the functions at different points of the region Ω.

When approximating the velocities, instead of the function f, it is necessary to substitute the values obtained by $\bar{v}_z$ or $\bar{v}_r$ from (47), then by getting f for the functions v_z and v_r, respectively.

When calculating velocities, weight factor $\alpha_1 = 1$. Empirically, $\delta = 0.01$ for v_z, and $\delta = 0.001$ for v_r.

Approximations for v_z and v_r are presented in the form of structures:

$$v_z = \sum_{k=1}^{k} c_k \left(\beta_k - r\frac{\partial \beta_k}{\partial r}\right); \quad (50)$$

$$v_r = \sum_{k=1}^{k} c_k \beta_k, \quad (51)$$

where c_k – arbitrary numerical coefficients; $\beta_k(z, r)$ – parameters of Schoenberg's B-splines.

Ratios (47) and (51) make it possible to satisfy the conditions of axial symmetry identically:

$$v_r = 0;\ \frac{\partial v_r}{\partial r} \neq 0;\ \frac{\partial v_z}{\partial r} \neq 0. \quad (52)$$

Substitution of structures (50) and (51) to (49) and minimization of the obtained expression by the coefficients of c_k leads to a system of linear algebraic equations with respect to c_k, where p-th equation has the following form:

$$\sum_{k=1}^{k} c_k \left\{\sum_{l=1}^{L} \alpha_l f_l(\beta_k) f_l(\beta_p) + \delta \iint_{\Omega} \left[\frac{\partial^2 f(\beta_k)}{\partial z^2}\frac{\partial^2 f(\beta_p)}{\partial z^2} + 2\frac{\partial^2 f(\beta_k)}{\partial z \partial r}\frac{\partial^2 f(\beta_p)}{\partial z \partial r} + \frac{\partial^2 f(\beta_k)}{\partial r^2}\frac{\partial^2 f(\beta_p)}{\partial r^2}\right] d\Omega\right\} = \sum_{l=1}^{L} \alpha_l \bar{f}_l f_l(\beta_p). \quad (53)$$

After substituting the values of c_k obtained after solving the system of equations in (50) and (51), the approximations v_z and v_r can be obtained.

The components of the strain rate tensor are determined according to equation (26). Simultaneously, they accepted as $\dot{e}_{11} = \dot{e}_z$, $\dot{e}_{12} = \dot{e}_{zr}$, $\dot{e}_{22} = \dot{e}_r$, $\dot{e}_{23} = \dot{e}_{31} = 0$, and $\dot{e}_{33} = \dot{e}_\phi$.

The accumulated deformation of the base material in the nodes of the coordinate grid at the mth stage is determined as follows:

$$\Gamma_{0_{l,m}} = \int_0^{t_m} \dot{\gamma}_{0_l}(t)dt. \quad (54)$$

To approximate functions $\dot{\gamma}_{0_l}(t_m)$ for $m = 0, 1, \ldots, 3$ and integrating them according to formula (54), cubic splines of one argument is used.

At the m-th stage, to obtain a continuous distribution of the accumulated strain $\Gamma_0(r, z)$ over the region Ω, the values at the nodes are obtained by formula (54) using the dependence (53) and assuming $\bar{f}_l = \Gamma_{0_{l,m}}$. For calculations, values $\alpha_1 = 1$ and $\delta = 0.01$ are taken. The structure is taken as follows:

$$\Gamma_0 = \sum_{k=1}^{k} c_k \left(\beta_k - r\frac{\partial \beta_k}{\partial r}\right). \quad (55)$$

Structure (55) provides the condition of axial symmetry.

This method of calculating Γ_0 is more suitable for non-stationary deformation, as it allows for considering the influence of the type of load trajectory.

However, the advantages of calculating the accumulated deformation of the base material Γ_0 according to the above method during the stationary course of the plastic deformation process are apparent.

After considering

$$\dot{e} = \frac{\dot{\theta}}{1-\theta} \quad (56)$$

and formulas (26), (30) and (32), the cross-sectional porosity distribution at each stage can be obtained as follows:

$$\theta = 1 - (1 - \theta_0)\left(\frac{\partial z_0}{\partial z}\frac{\partial r_0}{\partial r} - \frac{\partial z_0}{\partial r}\frac{\partial r_0}{\partial z}\right)\frac{r_0}{r}. \quad (57)$$

6 Conclusions

The experimental and computational methods of studying the stress-strain state during plastic deformation of porous bodies were improved. For this purpose, the advantages of the R-function theory were used.

As a result, an equation for calculating the porosity in the volume of the deformable workpiece was obtained, considering the information about the distortion of the dividing mesh elements.

For stationary axisymmetric processes, a technique has been developed that allows for replacing the calculation of the accumulated deformation of the base material Γ_0 along the deformation trajectory by integration over the area. This makes it possible to reduce the calculation error and simplify the algorithm.

Overall, a novel technique to determine the stress-strain state was developed at the unstable and steady stages of axisymmetric plastic deformation of porous blanks.

References

1. Grushko, A., Kukhar, V., Slobodyanyuk, Y. (2017). Phenomenological model of low-carbon steels hardening during multistage drawing. *Solid State Phenomena*, Vol. 265, pp. 114–123. https://doi.org/10.4028/www.scientific.net/SSP.265.114
2. Puzyr, R., Shchetynin, V., Vorobyov, V., Skoriak, Y., Negrebetskyi, I. (2021). Improving the technology for manufacturing hollow cylindrical parts for vehicles by refining technological estimation dependencies. *Eastern-European Journal of Enterprise Technologies*, Vol. 6(1(114)), pp. 56–64. https://doi.org/10.15587/1729-4061.2021.244241
3. Hrudkina, N., Markov, O., Shapoval, A., Titov, V., Aliyev, I., Abhari, P., Malii, K. (2022). Mathematical and computer simulation for the appearance of dimple defect by cold combined extrusion. *FME Transactions*, Vol. 50(1), pp. 90–98. https://doi.org/10.5937/fme2201090H
4. Hosford, W. F., Caddell, R. M. (2007). *Metal Forming: Mechanics and Metallurgy*. Cambridge University Press, Cambridge, UK.

5. Baldinozzi, G., Pontikis, V. (2022). Phenomenological potentials for the refractory metals Cr, Mo and W. *Journal of Physics: Condensed Matter*, Vol. 34(31), pp. 315–702. https://doi.org/10.1088/1361-648X/ac73ce
6. Jia, X., Hao, K., Luo, Z., Fan, Z. (2022). Plastic deformation behavior of metal materials: A review of constitutive models. *Metals*, Vol. 12(12), 2077. https://doi.org/10.3390/met12122077
7. Knudsen, T. (2008). *An Experimental Study of Plastic Deformation of Materials*. PhD thesis, Technical University of Denmark, Roskilde, Denmark.
8. Kronsteiner, J., Horwatitsch, D., Hinterer, A., Gusenbauer, C., Zeman, K. (2016). Experimental determination of plastic strain in the extrusion process. *AIP Conference Proceedings*, Vol. 1769, 140001. https://doi.org/10.1063/1.4963538
9. Kulagin, R., Beygelzimer, Y., Bachmaier, A., Pippan, R., Estrin, Y. (2019). Benefits of pattern formation by severe plastic deformation. *Applied Materials Today*, Vol. 15, pp. 236–241. https://doi.org/10.1016/j.apmt.2019.02.007
10. Prager, W., (1995). The theory of plasticity: A survey of recent achievements. *Proceedings of the Institution of Mechanical Engineers*, Vol. 169(1), pp. 41–57. https://doi.org/10.1243/PIME_PROC_1955_169_015_02
11. Versino, D., Tonda, A., Bronkhorst, C. A. (2017). Data driven modeling of plastic deformation. *Computer Methods in Applied Mechanics and Engineering*, Vol. 318, pp. 981–1004. https://doi.org/10.1016/j.cma.2017.02.016
12. Hah, Z.-H., Youn, S.-K. (2015). Eulerian analysis of bulk metal forming processes based on spline-based meshfree method. *Finite Elements in Analysis and Design*, Vol. 106, pp. 1–15. https://doi.org/10.1016/j.finel.2015.07.004
13. Schröder, J., Balzani, D., Brands, D. (2011). Approximation of random microstructures by periodic statistically similar representative volume elements based on lineal-path functions. *Archive of Applied Mechanics*, Vol. 81, pp. 975–997. https://doi.org/10.1007/s00419-010-0462-3
14. Gogaev, K. A., Voropaev, V. S., Podrezov, Yu. N., Lugovskoi, Yu. F., Nazarenko, V. A., Koval, A. Yu., Yevych, Ya. I. (2017). Mechanical and fatigue properties of powder titanium strips, obtained by asymmetric rolling. *Powder Metallurgy and Metal Ceramics*, Vol. 56(1–2), pp. 69–77. https://doi.org/10.1007/s11106-017-9871-y
15. Dell, H., Gese, H., Oberhofer, G. (2007). CrachFEM – A comprehensive approach for the prediction of sheet metal failure. *AIP Conference Proceedings*, Vol. 908, pp. 165–170. https://doi.org/10.1063/1.2740806
16. Veselovska, N., Shargorodsky, S., Rutkevych, V., Iskovych-Lototsky, R., Omiotek, Z., Mamyrbaev, O., Zhunissova, U. (2021). *Analysis of the Character of Change of the Profilogram of Micro Profile of the Processed Surface*. In: Mechatronic Systems II. Applications in Material Handling Processes and Robotics, pp. 165–174. Routledge Taylor & Francis Group, New York, NY, USA.
17. Papadopoulos, P., Lu, J. (2001). On the formulation and numerical solution of problems in anisotropic finite plasticity. *Computer Methods in Applied Mechanics and Engineering*, Vol. 190(37–38), pp. 4889–4910. https://doi.org/10.1016/S0045-7825(00)00355-8
18. Bašić, H., Demirdzic, I., Muzaferia, S. (2005). Finite volume method for simulation of extrusion processes. *International Journal for Numerical Methods in Engineering*, Vol. 62(4), pp. 475–494. https://doi.org/10.1002/nme.1168
19. Weselowska, N., Turych, V., Rutkevych, V., Ogorodnichuk, G. Kisała, P., Yeraliyeva, B., Yusupova, G. (2021). *Investigation of Interaction of a Tool with a Part in the Process of Deforming Stretching with Ultrasound*. In: Mechatronic Systems II. Applications in Material Handling Processes and Robotics, pp. 175–184. Routledge Taylor & Francis Group, New York, NY, USA.
20. Veselovska, N. R., Shargorodsky, S. A., Larysa, E. Nykyforova, L. E, Omiotek, Z., Baglan, I., Kozhamberdiyeva, M. (2022). *Efficiency Assessment Functioning of Vibration Machines for Biomass Processing*. In Biomass as Raw Material for Production of Biofuels and Chemicals, pp. 53–60. Routledge Taylor & Francis Group, London, UK.
21. Pokras, V, Rvachev, M. (1996). Application of the R-functions method to visioplastic analysis in metal forming. *Journal of Materials Processing Technology*, Vol. 60(1–4), pp. 493–500. https://doi.org/10.1016/0924-0136(96)02376-X
22. Ogorodnikov, V. A., Dereven'ko, I. A., Sivak, R. (2018). On the influence of curvature of the trajectories of deformation of a volume of the material by pressing on its plasticity under the conditions of complex loading. *Materials Science*, Vol. 54(3), pp. 326–332. https://doi.org/10.1007/s11003-018-0188-x
23. Nalobina, O. O., Vasylchuk, N. V., Bundza, O. Z., Holotiuk, M. V., Veselovska, N. R., Zoshchuk, N. V. (2019). A new technical solution of a header for sunflower harvesting. *INMATEH-Agricultural Engineering*, Vol. 58(2), pp. 129–136.
24. Shatokhin, V., Ivanchuk, Y., Dvirna, O., Veselovskaya, N., Jurczak, W. (2022). Dynamic processes modeling in a peristaltic pump with a hydraulic drive for the Bingham fluid. *Advances in Science and Technology Research Journal*, Vol. 16(4), pp. 256–269. https://doi.org/10.12913/22998624/152944
25. Sivak, R., Kulykivskyi, V., Savchenko, V., Minenko, S., Borovskyi, V. (2023). Determination of porosity functions in the pressure treatment of iron-based powder materials in agricultural engineering. *Scientific Horizons*, Vol. 26(3), pp. 124–134. https://doi.org/10.48077/scihor3.2023.124
26. Shtern, M., Mikhailov, O., Mikhailov, A. (2021). Generalized continuum model of plasticity of powder and porous materials. *Powder Metallurgy and Metal Ceramics*, Vol. 60(1–2), pp. 20–34. https://doi.org/10.1007/s11106-021-00211-7
27. Aliyeva, L., Hrudkina, N., Aliyev, I., Zhbankov, I., Markov, O. (2020). Effect of the tool geometry on the force mode of the combined radial-direct extrusion with compression. *Eastern-European Journal of Enterprise Technologies*, Vol. 2(1(104)), pp. 15–22. https://doi.org/10.15587/1729-4061.2020.198433